Ezh2 maintains a key phase of muscle satellite cell expansion but does not regulate terminal differentiation

Samuel Woodhouse*, Dhamayanthi Pugazhendhi‡, Patrick Brien and Jennifer M. Pell‡,§

The Babraham Institute, Cambridge, CB22 3AT, UK

*Present address: Centre for Stem Cells and Regenerative Medicine, Kings College London, London SE1 9RT, UK
‡Present address: Department of Pharmacology, University of Cambridge, Tennis Court Road, Cambridge CB2 1PD, UK
§Author for correspondence (jp373@cam.ac.uk)

Accepted 2 November 2012
Journal of Cell Science 126, 565–579

doi: 10.1242/jcs.114843

Summary

Tissue generation and repair requires a stepwise process of cell fate restriction to ensure that adult stem cells differentiate in a timely and appropriate manner. A crucial role has been implicated for Polycomb-group (PcG) proteins and the H3K27me3 repressive histone mark in coordinating the transcriptional programmes necessary for this process, but the targets and developmental timing for this repression remain unclear. To address these questions, we generated novel genome-wide maps of H3K27me3 and H3K4me3 in freshly isolated muscle stem cells. These data, together with the analysis of two conditional Ezh2-null mouse strains, identified a critical proliferation phase in which Ezh2 activity is essential. Mice lacking Ezh2 in satellite cells exhibited decreased muscle growth, severely impaired regeneration and reduced stem cell number, due to a profound failure of the proliferative progenitor population to expand. Surprisingly, deletion of Ezh2 after the onset of terminal differentiation did not impede muscle repair or homeostasis. Using these knockout models and the RNA-Seq and ChIP-Seq datasets, we show that Ezh2 does not regulate the muscle differentiation process *in vivo*. These results emphasise the lineage and cell-type-specific functions of Ezh2 and Polycomb repressive complex 2.

Key words: ChIP-Seq, Ezh2, H3K27me3, Muscle stem cells, PRC2, Satellite cell

Introduction

Maintenance of a correct differentiation programme is essential for tissue homeostasis and repair. Accumulating evidence suggests that the Polycomb group (PcG) proteins, which mediate transcriptionally repressive epigenetic information, represent likely candidates for the regulation of adult stem cell fate and differentiation. Polycomb repressive complex 2 (PRC2) is composed of four core subunits, Ezh2, Suz12, EED and RbAp48, with Ezh2 responsible for the trimethylation of lysine 27 of histone H3 (H3K27me3) (Margueron et al., 2008; Shen et al., 2008). Numerous studies investigating embryonic stem cells (ESCs) have demonstrated that PRC2 and H3K27me3 transcriptionally repress key factors involved in lineage specification (which are de-repressed in PRC2-deficient ESCs) leading to aberrant differentiation programs (Boyer et al., 2006; Chamberlain et al., 2008; Leeb et al., 2010; Mikkelsen et al., 2007; Pan et al., 2007; Pasini et al., 2007; Pasini et al., 2010; Shen et al., 2008; Wang et al., 2008). In ESCs, genes encoding key developmental regulators have been suggested to contain multiple histone modifications, i.e. the repressive H3K27me3 mark and a histone mark associated with gene transcription, H3K4me3. These 'bivalent' domains are thought to poise these factors for rapid expression or repression (Bernstein et al., 2006; Mikkelsen et al., 2007; Vastenhouw and Schier, 2012).

The ability to study the function of PRC2 within an adult stem cell population has been hampered by the prenatal lethality of *Eed*, *Suz12* and *Ezh2* null embryos (Faust et al., 1995; O'Carroll et al., 2001; Pasini et al., 2004; Schumacher et al., 1996). Conditional deletion of Ezh2, for example, in B cells (Su et al., 2003), neuronal stem cells (Hirabayashi et al., 2009; Pereira et al., 2010), epidermal progenitors (Ezhkova et al., 2011; Ezhkova et al., 2009; Lien et al., 2011) and pancreatic islet β cells (Chen et al., 2009) has provided insights into the function of PRC2 within lineage restricted somatic cells. However, the differing phenotypes within these studies indicate that Ezh2 action may be highly dependent on the differentiation stage of the stem cell and may even regulate the differentiation programme (Benoit et al., 2012). Interestingly, loss of Ezh2 within cardiac progenitors leads to an upregulation of Six1 dependent skeletal muscle genes (Delgado-Olguín et al., 2012), suggesting that Ezh2 may not only be required for stem cell function but may also act to ensure the correct lineage choice of a stem cell.

The process of skeletal muscle development and repair serves as an excellent paradigm with which to investigate adult stem cell self-renewal, lineage specification and terminal differentiation. Skeletal muscle has a high regenerative capacity, with satellite cells (the principal muscle stem cell) being responsible for this capability (Lepper et al., 2011; Murphy et al., 2011; Sacco et al., 2008; Sambasivan et al., 2011). The mechanisms that govern the lineage restricted nature of these stem cells, and the fate choice to either differentiate or self-renew, have until recently been studied in the C2C12 myoblast cell line, which is thought to recapitulate the differentiation programmes that occur *in vivo*. Indeed, using the C2C12 cell line, Ezh2 has been suggested to be a master

Journal of Cell Science

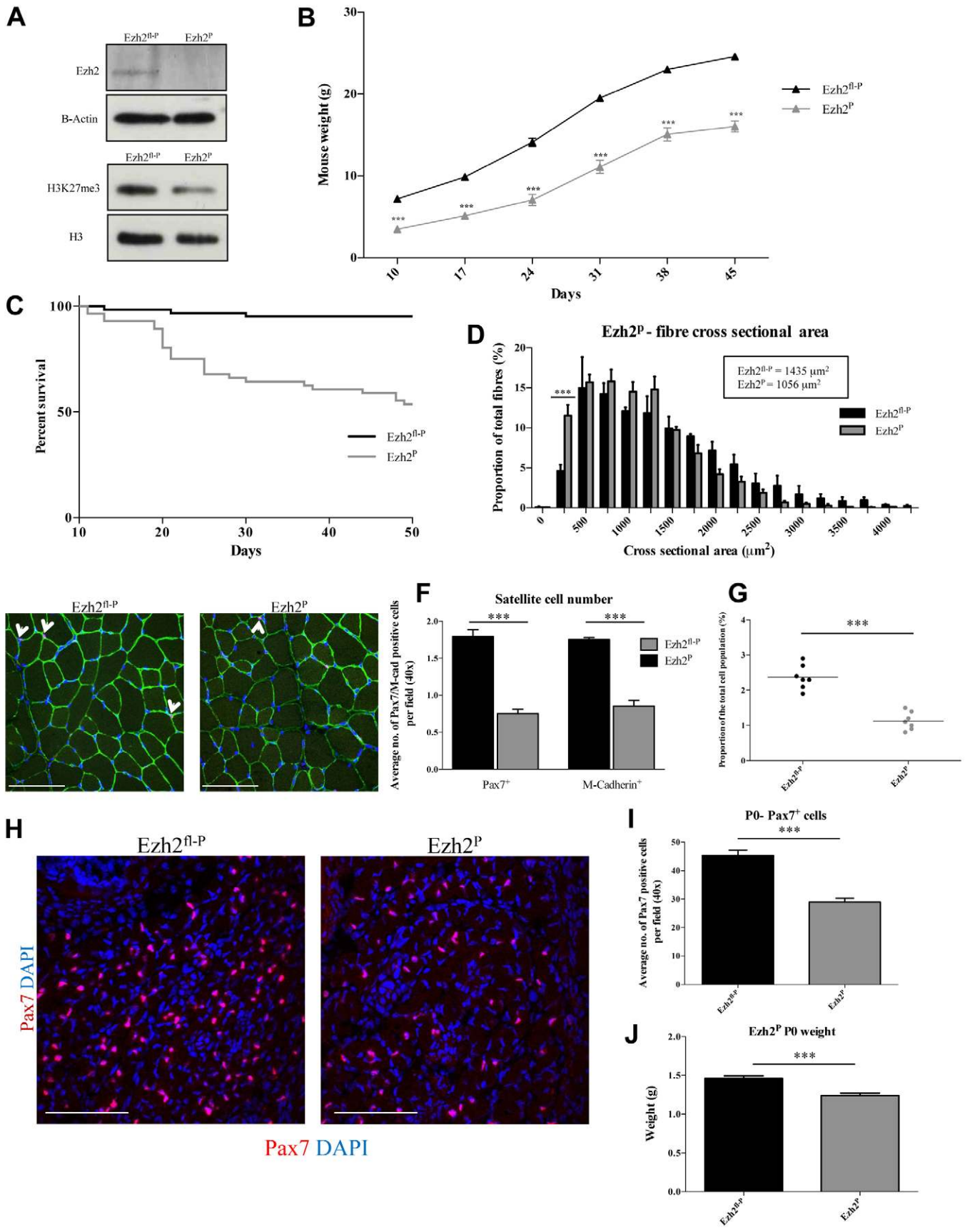

Fig. 1. See next page for legend.

regulator of the muscle terminal differentiation process by suppressing key muscle differentiation genes (Juan et al., 2009; Palacios et al., 2010; Seenundun et al., 2010). Recently, Juan et al. (Juan et al., 2011) suggested that loss of Ezh2 in $Pax7^+$ satellite cells causes defects in stem cell self-renewal, although the role of Ezh2 within the terminal differentiation process was not addressed in this study. Surprisingly, expression profiling from the Ezh2 null skeletal muscle tissue (a mixed population of differentiated muscle and non-myogenic cells) showed only small changes in gene expression patterns (123 upregulated transcripts, with the majority only two-fold higher than controls) (Juan et al., 2011). However, studies utilising the C2C12 cell line have shown that over 4,000 gene promoters are marked by H3K27me3 (Asp et al., 2011). Indeed, siRNA-mediated depletion of Ezh2 or Suz12 in C2C12 cells leads to enhanced muscle differentiation and upregulation of muscle differentiation genes (Asp et al., 2011; Juan et al., 2009).

In this study, we use knockout models and genome wide datasets to define the myogenic cell population in which Ezh2 functions, and to determine categorically if Ezh2 regulates the terminal differentiation process *in vivo*. By coupling these observations with genome-wide mapping of H3K27me3 and H3K4me3 in isolated primary satellite cells, we identify a fundamental role for H3K27me3 in suppressing factors associated with lineage specification within a proliferative progenitor population. This approach has identified that Ezh2 does not function during the terminal differentiation process or regulate terminal differentiation genes.

Results

Deletion of Ezh2 within satellite cells impairs muscle growth and survival

We characterised the functional consequence of deleting Ezh2 within the satellite cell pool using a Pax7-Cre ($Ezh2^P$ strain). Skeletal muscle derived from the $Ezh2^P$ mouse line exhibited an absence of Ezh2 protein and a global reduction in H3K27me3 at 7 weeks of age (Fig. 1A). In agreement with Juan et al. (Juan et al., 2011), the $Ezh2^P$ mouse line exhibited significant growth retardation (Fig. 1B), which was in large part due to a decrease in muscle fibre area (Fig. 1D,E) and subsequent reduction in muscle mass (supplementary material Fig. S1A). However, in contrast to previous work, we observed a high degree of postnatal lethality – only 54% of $Ezh2^P$ mice survived until P50 (Fig. 1C). The $Ezh2^P$ line is on a C57/B6 background, which may account for the lethality differences observed between this study and that of Juan et al. (Juan et al., 2011). Loss of Ezh2 within the satellite cell lineage has been suggested to lead to a decline in satellite cell number (Juan et al., 2011). We also observed these defects, with a 65% reduction in the number of $Pax7^+$ or M-Cadherin$^+$ (two well-characterised satellite cell markers) satellite cells (Fig. 1E,F). This was confirmed by FACS analysis, with a 63% reduction in $Vcam1^+$ $CD34^+$ $CD31^-$ $CD45^-$ satellite cells in limb skeletal muscle (Fig. 1G). During embryonic development and early postnatal growth $Pax7^+$ progenitor cells expand rapidly and are required to establish the quiescent satellite cell pool that is maintained throughout adult life (White et al., 2010). We therefore reasoned that the reduction in satellite cell number observed could occur during the establishment of the quiescent satellite cell population. Indeed, at P0 we observed a 15% reduction in mouse weight and a 40% reduction in $Pax7^+$ progenitors in skeletal muscle (Fig. 1H–J), demonstrating that some of the lesions in the $Ezh2^P$ line are established prenatally. However, $Ezh2^P$ mice are born at Mendelian ratios (25 expected, 22 obtained), which is in contrast to the lethality that occurs postnatally (Fig. 1C). Additionally, the growth defect is exacerbated after birth, with $Ezh2^P$ mice being 50% smaller than littermates by P10 (Fig. 1B).

Fig. 1. Conditional knockout of Ezh2 impairs skeletal muscle growth. (**A**) Western blot for Ezh2 (β-actin control) and H3K27me3 (total H3 control). $Ezh2^{fl\text{-}P}$, Ezh2 fl/fl without Pax7-Cre; $Ezh2^P$, Ezh2 fl/fl with Pax7-Cre. (**B**) Whole-body mouse weights (male); means±s.e.m.; $n=11$ per time point. ***$P<0.001$, significantly different from $Ezh2^{fl\text{-}P}$, assessed by ANOVA. (**C**) Kaplan–Meier survival curves for the knockout mouse strains; $Ezh2^P$, $n=35$; $Ezh2^{fl\text{-}P}$, $n=56$. (**D**) Proportion of myofibres per cross-sectional area (CSA) for the $Ezh2^P$ strain (700 myofibres assessed per n; $n=3$); mean CSA is shown. (**E**) Pax7 and laminin staining of cross-sections of TA muscle; nuclei are counterstained with DAPI (blue); arrowheads indicate $Pax7^+$ cells. Scale bars: 100 µm. (**F**) Quantification of the average number of Pax7- or M-cadherin-positive cells Scale bars: 100 µm. per field of view (40×); means+s.e.m.; $n=3$. (**G**) Flow cytometry analysis of the proportion of $Vcam1^+$ $CD34^+$ $CD31^-$ $CD45^-$ satellite cells within a satellite cell preparation derived from limb skeletal muscle; percentage calculated from a total of 300,000 events per sample; independent observations are shown. (**H**) Pax7 staining (red) in cross-sections of newborn (P0) hind leg. DAPI (blue) is used to mark nuclei. Scale bars: 100 µm. (**I**) The average number of $Pax7^+$ cells per field of view (40×) is significantly reduced in the newborn (P0) $Ezh2^P$ mice. Means+s.e.m.; $n=3$. **$P<0.01$ assessed by Student's t-test. (**J**) $Ezh2^P$ mice are significantly smaller than littermate controls at birth (P0); means+s.e.m.; $Ezh2^P$ $n=8$, $Ezh2^{fl\text{-}P}$ $n=17$; ***$P<0.001$ assessed by Student's t-test.

Ezh2 is required for muscle regeneration but not satellite cell self-renewal

The $Ezh2^P$ defects (Fig. 1H–J) suggest that the phenotype observed in the adult could be due to a failure to expand the progenitor population during development. To directly test whether or not Ezh2 has a role in satellite cell self-renewal, we employed a muscle regeneration protocol, which measures the ability of stem cells to repair skeletal muscle and maintain the stem cell population. Muscle regeneration was assessed 5 (early phase of repair), 10 (late phase of repair) and 25 (fully regenerated) days following cardiotoxin (CTX)-induced muscle damage. Muscle regeneration was nearly completely absent from the $Ezh2^P$ mice 25 days post CTX injection – only a small number of centrally nucleated fibres (a hallmark of newly formed myofibres) were observed (Fig. 2A,B). This failure to regenerate was accompanied by an accumulation of calcium deposits (Alizarin Red), fatty deposits (Oil Red O) and fibrous tissue (Van Gieson) (Fig. 2A). By analysing regeneration across a time course we were able to show that Ezh2 is required for effective muscle regeneration and does not simply delay muscle repair, as had been suggested by analysis of the tissue at 7 days after CTX injection (Juan et al., 2011).

During regeneration satellite cells expand in response to injury, repair the damaged area and return to a quiescent state to ensure the maintenance of the stem cell pool (Shea et al., 2010). Using the CTX regeneration model it is therefore possible to examine stem cell self-renewal *in vivo*. The number of $Pax7^+$ cells was quantified during the regeneration time course (Fig. 2C,D). As expected, the number of $Ezh2^{fl\text{-}P}$ satellite cells increased ninefold in response to the regenerative stimulus, returning to baseline by 25 days after injury. However, Ezh2 null $Pax7^+$ cells were unable to expand during regeneration and their number remained at

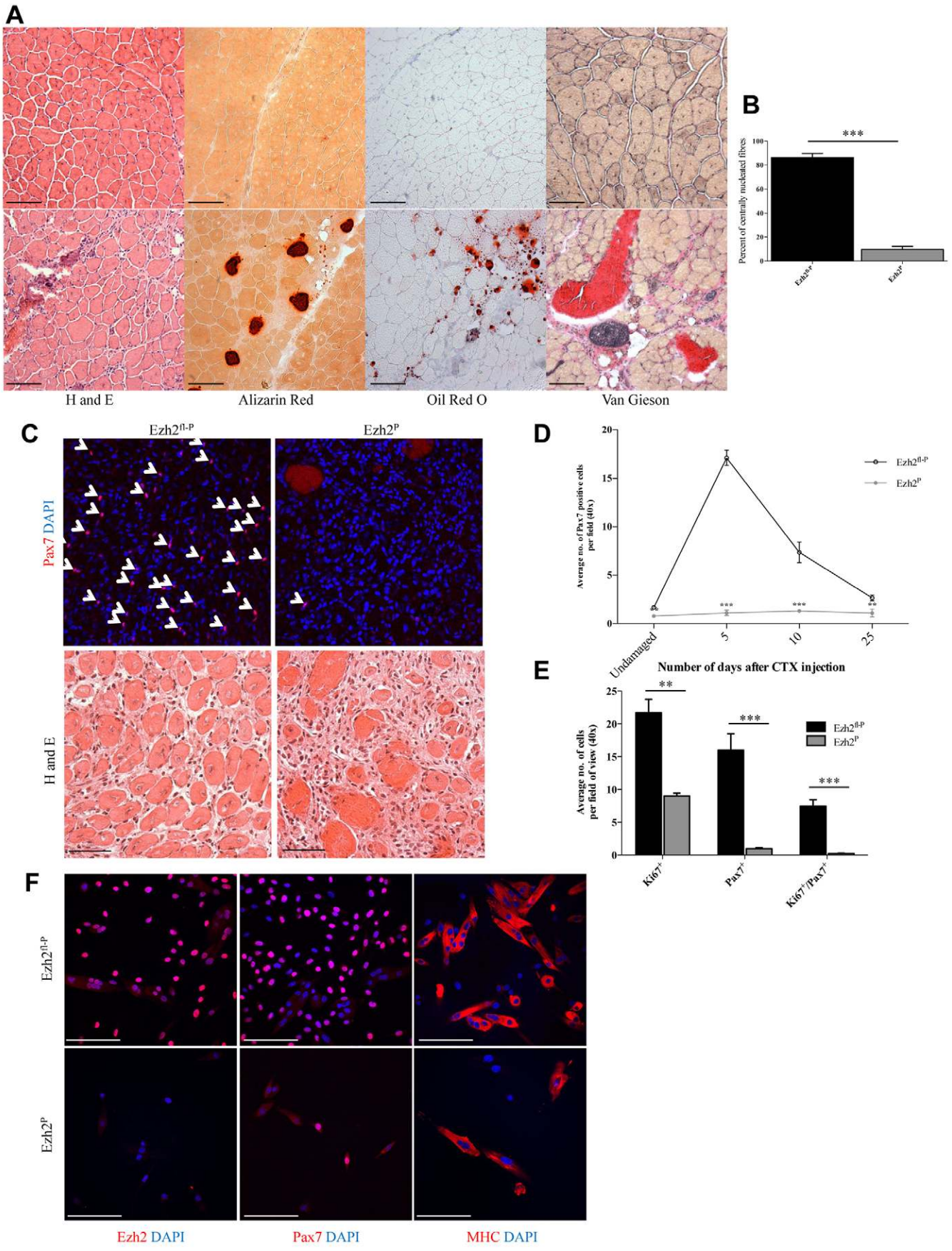

Fig. 2. See next page for legend.

pre-regeneration levels (Fig. 2D). This failure to expand in response to regenerative signals is due to significantly reduced proliferation, as indicated by $Ki67^+$ nuclei (Fig. 2E). No increase in apoptosis was observed, as determined by cleaved caspase 3 staining (supplementary material Fig. S1B). Crucially, the numbers of Ezh2 null satellite cells had not declined following the regeneration period (25 days).

These conclusions were also confirmed *ex vivo*. Ezh2 null satellite cells were isolated by FACS and cultured to induce activation, proliferation and differentiation. Following culture for 120 h after isolation, $Ezh2^P$ satellite cells showed a dramatic reduction in myoblast ($Pax7^+$) number (Fig. 2F). However, Ezh2 null satellite cells were still capable of undergoing terminal differentiation (MHC^+).

Ezh2 is not required for terminal differentiation or myofibre homeostasis

Without the actions of Ezh2 within $Pax7^+$ progenitors there is a severe defect in muscle growth and regeneration. This appears to be due to the failure of the progenitor cells to expand and thus supply the progeny for terminal differentiation, although it could be the result of a defect during the terminal differentiation process. Indeed, Ezh2 is expressed during muscle terminal differentiation, albeit at reduced levels (supplementary material Fig. S2A–C). Consequently, we set out to further characterise the developmental window in which Ezh2 and H3K27me3 exert their influence. To achieve this, a second conditional mouse line was generated by crossing Myogenin-Cre mice (Li et al., 2005) with the Ezh2 fl/fl strain, termed $Ezh2^M$. This specifically deleted Ezh2 at the onset of terminal differentiation, leaving the quiescent satellite cell and proliferating $MyoD^+$ populations intact. Skeletal muscle derived from the $Ezh2^M$ mouse line exhibited an absence of Ezh2 protein, and interestingly, a global reduction in H3K27me3 levels (Fig. 3A). The results observed in the $Ezh2^P$ mice were in marked contrast to the phenotype of the $Ezh2^M$ mice, which showed no defect in total body weight, fibre size or survival (Fig. 3B,C; data not shown). The number of satellite cells, the ability of $Ezh2^M$ skeletal muscle to regenerate (5–25 days) and the self-renewal of the satellite cell population was comparable to the $Ezh2^{fl\text{-}M}$ controls (Fig. 3D–F). Thus, importantly, it can be concluded that the phenotype observed in the $Ezh2^P$ line was due to intrinsic defects within myoblast populations prior to the onset of terminal differentiation. Consequently, the $Ezh2^P$ phenotype was not due to a deficiency in terminal differentiation, myoblast fusion or myofibre hypertrophy.

Fig. 2. Severely impaired muscle regeneration in Ezh2 null muscle. (**A**) Cross-sections of TA muscle taken from the $Ezh2^P$ strain 25 d after CTX injection and stained for haematoxylin and eosin (H and E), Alizarin Red (red/brown marks calcium deposits), Oil Red O (fat accumulation is marked in red) and Van Gieson (highlights fibrous tissue in red/pink), as indicated. Scale bars: 100 µm. (**B**) Proportion of muscle fibres within the damaged area with centralised nuclei. Means+s.e.m.; $n=3$. $^{***}P<0.001$, assessed by Student's *t*-test. (**C**) Cross-section of a damaged area 5 days after cardiotoxin injection stained for Pax7 (progenitor cells) or haematoxylin and eosin (H and E), as indicated; nuclei are counterstained with DAPI (blue). Scale bars: 100 µm. (**D**) The average number of $Pax7^+$ cells was determined from muscle sections; undamaged, 5, 10 and 25 days after CTX injection; means±s.e.m.; $n=3$. $^{**}P<0.01$, $^{***}P<0.001$, significantly different from $Ezh2^{fl\text{-}P}$, assessed by ANOVA. (**E**) Ki67 was used to quantify proliferating cells in the $Ezh2^P$ strain; the average number of $Ki67^+$, $Pax7^+$ and double-positive cells was quantified within a field of view (40×) 5 days after CTX injection; means+s.e.m.; $n=3$. $^{**}P<0.01$, $^{***}P<0.001$, assessed by Student's *t*-test. (**F**) FACS isolated satellite cells cultured for 120 h, stained for Ezh2, Pax7 and MHC; nuclei were counterstained with DAPI (blue). Scale bars: 100 µm.

Genome-wide mapping of H3K27me3 and H3K4me3 in muscle satellite cells

The known targets of Ezh2 in stem cells, is limited to hair follicle stem cells (Lien et al., 2011) and haematopoietic stem cells (HSCs) (Adli et al., 2010; Cui et al., 2009), with little information regarding the skeletal muscle lineage. We therefore set out to determine the genomic targets of Ezh2 and the interplay between repressive (H3K27me3) and active (H3K4me3) histone modifications in satellite cells. We optimised a flow-cytometry purification protocol (Fukada et al., 2007) to isolate a near pure population of satellite cells (Fig. 4A). The majority of isolated cells expressed the muscle stem cell markers Pax7 (92±3%; $n=3$; Fig. 4B) and M-cadherin (93%+5%; $n=3$). We developed a chromatin immunoprecipitation protocol for FACS isolated muscle satellite cells and performed next generation sequencing (ChIP-Seq), which was used to characterise the localisation of H3K4me3 and H3K27me3 within the satellite cell genome (supplementary material Tables S1 and S2, respectively). The majority (96%) of H3K4me3 regions were in close proximity (<2 kb) to annotated genes. H3K27me3 peaks were distributed broadly throughout the genome, with 57% of enriched regions in close proximity (<2 kb) to annotated genes. We validated the ChIP-Seq data sets by examining H3K4me3 and H3K27me3 regions with different levels of enrichment and performed independent ChIP analysis coupled to quantitative PCR (ChIP-qPCR; Fig. 4C,D).

Known satellite cell factors *Itga7*, *Ncam1*, *Cxcr4*, *Pax7* and *Myf5* (Fig. 4E; supplementary material Table S1) were enriched for the active histone modification H3K4me3. Furthermore, factors that have been proposed to regulate satellite cell function, *Sprouty1* (Shea et al., 2010), *Notch1* (Brack et al., 2008) and *Sox8* (Schmidt et al., 2003), were also marked by H3K4me3 (Fig. 4E), suggesting that our data set may provide a useful resource of novel regulators of satellite cell function that could be examined in future functional studies (supplementary material Table S1).

Within the satellite cell genome, H3K4me3 was found within 1 kb of the transcriptional start site (TSS) (Fig. 4F). The H3K27me3 repressive mark was distributed broadly around promoters and deep into gene bodies (Fig. 4F). While this is in contrast to the distribution seen in ESC cells, where there is a peak of H3K27me3 at TSS of genes (Bernstein et al., 2006; Boyer et al., 2006; Guttman et al., 2009; Mikkelsen et al., 2007; Pan et al., 2007; Wang et al., 2008), it mirrors the localisation observed in more lineage restricted cell types, including fibroblasts and $CD4^+$ T cells (Barski et al., 2007; Hawkins et al., 2010). The reduction in sequencing reads around the TSS observed for both H3K27me3 and input samples is a typical feature of ChIP-Seq studies (Asp et al., 2011; Barski et al., 2007; Cui et al., 2009; Pan et al., 2007; Young et al., 2011; Zhao et al., 2007), and most likely occurs due to the difficulties of sequencing GC rich TSSs.

In pluripotent ESCs, many genes encoding key developmental regulators are bivalent (Bernstein et al., 2006). However, we identified only 83 putative 'bivalent' domains within the satellite cell genome (supplementary material Table S3), supporting the notion that although bivalent domains may be a key feature of the

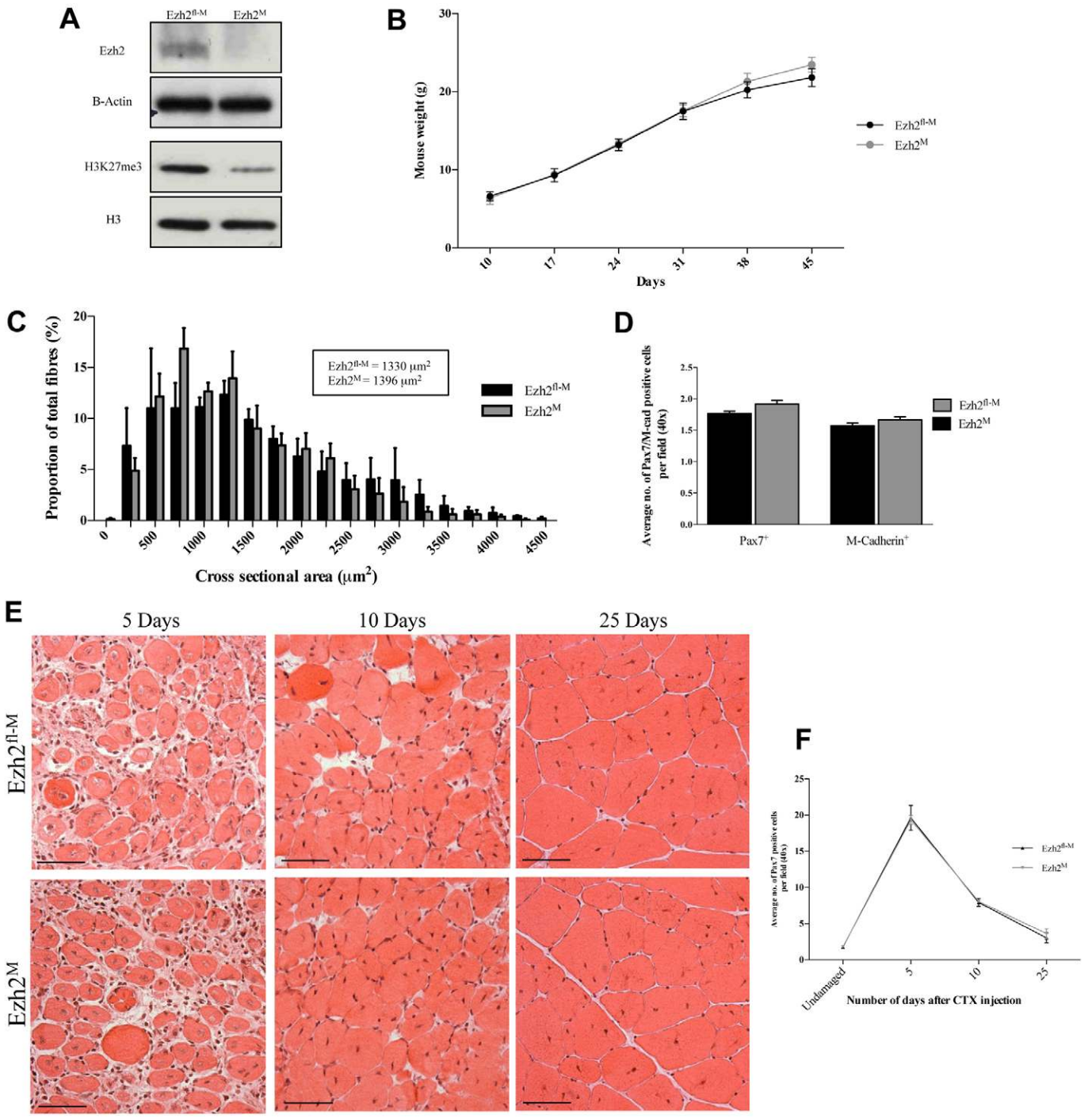

Fig. 3. Conditional knockout of Ezh2 during terminal differentiation. (**A**) Western blot for Ezh2 (with a β-actin control) and H3K27me3 (with a total H3 control). $Ezh2^{fl\text{-}M}$, Ezh2 fl/fl without Myogenin-Cre; $Ezh2^{M}$, Ezh2 fl/fl with Myogenin-Cre. (**B**) Whole-body mouse weights (male); means±s.e.m.; $n=5$ per time point. (**C**) Proportion of myofibres per cross-sectional area (CSA) for the $Ezh2^{M}$ strain (700 myofibres assessed per n, $n=3$); mean CSA is shown. (**D**) Quantification of the average number of Pax7- or M-cadherin-positive cells per field of view (40×); means+s.e.m.; $n=3$. (**E**) Haematoxylin and eosin staining of cross-sections of the TA muscle from the $Ezh2^{M}$ strain after injection of cardiotoxin (CTX). Muscle was harvested at 5, 10 and 25 days after injection. Scale bars: 100 µm. (**F**) The average number of $Pax7^{+}$ cells was determined from muscle sections; undamaged, 5, 10 and 25 days after CTX injection; means±s.e.m.; $n=3$.

ESC cell genome (containing >1600 bivalent domains), they may not be prevalent in the genome of the lineage-restricted satellite cell. GO ontology analysis on the bivalent domains (supplementary material Fig. S3B) indicated only a small enrichment for GO terms, suggesting that the bivalent domains that we identified do not share a common function.

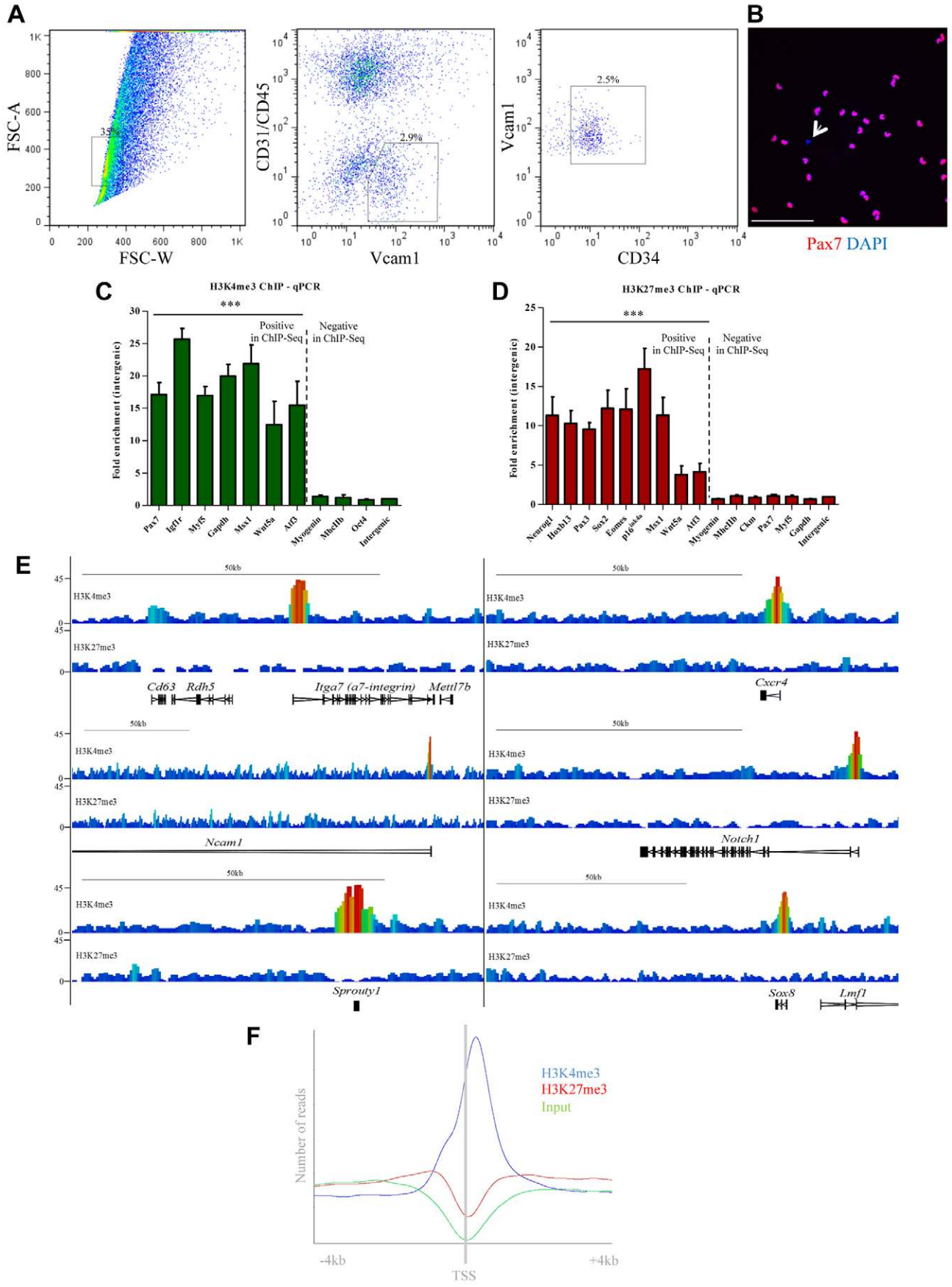

Fig. 4. See next page for legend.

H3K27me3 marks regulators of cell fate

The H3K27me3 mark was classically described as regulating the Hox clusters (Duncan, 1982; Soshnikova and Duboule, 2008) and this is also the case for muscle satellite cells, with broad H3K27me3 domains spread across Hox clusters (Fig. 5A). In the satellite cell population, H3K27me3 was also found at known non-myogenic cell fate regulators and genes associated with early development (examples are shown in Fig. 5B; GO analysis, Fig. 5C). However, factors involved in muscle development were not enriched in the H3K27me3 Gene Ontology (GO) analysis. By contrast, GO analysis indicated that the H3K4me3 was enriched at genes involved in muscle organ development and cellular homeostasis (Fig. 5D). Network analysis on the factors involved in muscle organ development suggests that there is crosstalk between these genes (supplementary material Fig. S3B). H3K27me3 was highly enriched at key transcription factors that regulate lineage decisions, such as members of the *Pax*, *Sox*, *Gata* and *Foxo* families (Fig. 5B; supplementary material Table S2); indeed all Pax transcription factors (Pax1–9), apart from Pax7, were marked by H3K27me3. Thus, in muscle stem cells, H3K27me3 is enriched at key developmental regulators associated with non-muscle lineages.

H3K27me3 and satellite cell identity

Our ChIP-Seq analysis identified that H3K27me3 marks a considerable number of key regulators of non-muscle development (Fig. 5B,C). Upon loss of Ezh2 there is a reduction of H3K27me3 at the promoters of *Neurog1* (neuronal differentiation and cell type specification), *Hoxb13* (foetal skin development), *Gata4* (myocardial differentiation) and *p16Ink4a* (Fig. 6A). No statistically significant enrichment of H3K4me3 was observed for these loci (supplementary material Fig. S5).

To determine transcriptome changes that occur upon the loss of Ezh2 and subsequent reduction of H3K27me3, we performed RNA-Seq analysis on Ezh2 null FACS isolated satellite cells. We observed significant upregulation of a number of transcripts within the $Ezh2^{P}$ strain compared to the $Ezh2^{Fl\text{-}P}$ strain (supplementary material Table S4). We also noted a considerable number of transcripts that had low sequence reads (corresponding to low/no expression) in $Ezh2^{fl\text{-}P}$ satellite cells, but which showed greater than twofold increase in the $Ezh2^{P}$ satellite cells (Fig. 6B). However, only 11.4% (71/624) of the genes marked by H3K27me3 in satellite cells were upregulated greater than twofold in Ezh2 null satellite cells (Fig. 6B). Interestingly, these genes corresponded to factors involved in the mesenchymal lineage, cell fate commitment and transcription factor activity. Genes marked by H3K27me3 and not upregulated upon Ezh2 loss, were also highly enriched for factors involved in cell fate commitment. However, a significant proportion was associated with factors involved in embryonic morphogenesis, epithelium development and kidney development – i.e. lineages that are very distinct from the skeletal muscle lineage (Fig. 6B). Thus, the RNA-Seq analysis suggests that only a proportion of the genes marked by H3K27me3 in satellite cells are suppressed by this modification. Instead, it implies that a large proportion of H3K27me3 marked genes may be suppressed by further layers of epigenetic repression or may require transcriptional machinery that is not present in the satellite cell.

To further examine the global consequences of Ezh2 loss we performed network and GO analysis on the transcripts upregulated in $Ezh2^{P}$ satellite cells. The upregulated transcripts have diverse functions (Fig. 6B), although a significant proportion ($P=8.3E\text{-}7$) were involved in cell cycle regulation (Fig. 6C). The phenotype of the $Ezh2^{P}$ strain suggested that Ezh2 may suppress factors involved in cell cycle progression. One such locus, the *Cdkn2a* locus, has been identified as a key target of Ezh2 within pancreatic islet β cells (Chen et al., 2009), epidermal stem cells (Ezhkova et al., 2011; Ezhkova et al., 2009) and numerous cancers (Agger et al., 2009; Barradas et al., 2009). Indeed, the only cyclin dependent kinase (CDK) inhibitor marked by H3K27me3 in wild-type satellite cells is $p16^{Ink4a}$ (Fig. 4D; Fig. 7A), which is encoded by the *Cdkn2a* locus. Interestingly, in Ezh2 null satellite cells ($Ezh2^{P}$) the *Cdkn2a* locus exhibited a 70% reduction in H3K27me3 enrichment when compared with wild-type ($Ezh2^{fl\text{-}P}$) (Fig. 6A). This loss of H3K27me3 was accompanied by a considerable increase in $p16^{Ink4a}$ and $p19^{Arf}$ mRNA levels (Fig. 7B).

Ezh2 and H3K27me3 do not suppress muscle terminal differentiation genes

By combining the ChIP-Seq data set with RNA-Seq and RT-qPCR (Fig. 6C) analysis of the Ezh2 null satellite cells, we were able to determine whether Ezh2 suppresses myoblast terminal differentiation. Surprisingly, our ChIP-Seq study shows that H3K27me3 does not in fact mark key muscle differentiation genes in satellite cells. We determined that *MhcIIb*, *Myogenin* and *Ckm* were marked in C2C12 cells (supplementary material Fig. S2B), but no H3K27me3 enrichment was detected by ChIP-Seq (Fig. 7C) or ChIP-qPCR (Fig. 4D) on freshly isolated satellite cells. Importantly, loss of Ezh2 in satellite cells does not lead to an upregulation of Myogenin, Ckm or MhcIIb transcripts (Fig. 7B). GO analysis on the RNA-seq data set indicates that genes associated with muscle development/differentiation are not significantly ($P=0.5$) upregulated in Ezh2 null satellite cells (Fig. 6B).

To confirm these results we examined the capability of Ezh2 null satellite cells to commit to terminal differentiation both *ex vivo* and *in vivo*. FACS purified $Ezh2^{P}$ satellite cells committed to the terminal differentiation programme (as marked by Myogenin expression) at an equivalent rate to the $Ezh2^{fl\text{-}P}$ controls (Fig. 7D). These results were mirrored *in vivo* – resting muscle of either $Ezh2^{fl\text{-}P}$ or $Ezh2^{P}$ mice showed no expression of Myogenin (Fig. 7E). Additionally, the defects within the progenitor population led to a 70% reduction in $Myogenin^{+}$ cells in the $Ezh2^{P}$ line during muscle regeneration (Fig. 7F).

Fig. 4. ChIP-Seq on satellite cells. (**A**) Representative FACS plots for the isolation of satellite cells. The final cell population is $DAPI^{-}$ $CD31^{-}$ $CD45^{-}$ $Vcam1^{+}$ $CD34^{+}$. A total of 30,000 events are shown; gates are set according to single-stained controls. (**B**) FACS-isolated cells were cytospun, and immunofluorescence for Pax7 (red) was performed; nuclei are marked by DAPI staining (blue). The arrowhead indicates a $Pax7^{-}$ cell. (**C**,**D**) ChIP-qPCR for indicated gene promoters, for H3K4me3 (C) or H3K27me3 (D); chromatin was obtained from freshly isolated satellite cells; data are normalised to input and presented as fold enrichment relative to an intergenic region on chromosome 1 (intergenic); means±s.e.m; H3K4me3, $n=3$; H3K27me3, $n=4$. ***$P<0.001$, significantly different from *Oct4* (H3K4me3) or *Gapdh* (H3K27me3), assessed by ANOVA. (**E**) Read-density plot for *a7-integrin, Cxcr4, Ncam1, Notch1, Sprouty1* and *Sox8*. Peaks indicate read density. (**F**) Plot for the average read density±4 kb of the transcriptional start site (TSS) of all annotated genes; H3K4me3, blue; H3K27me3, red; input, green.

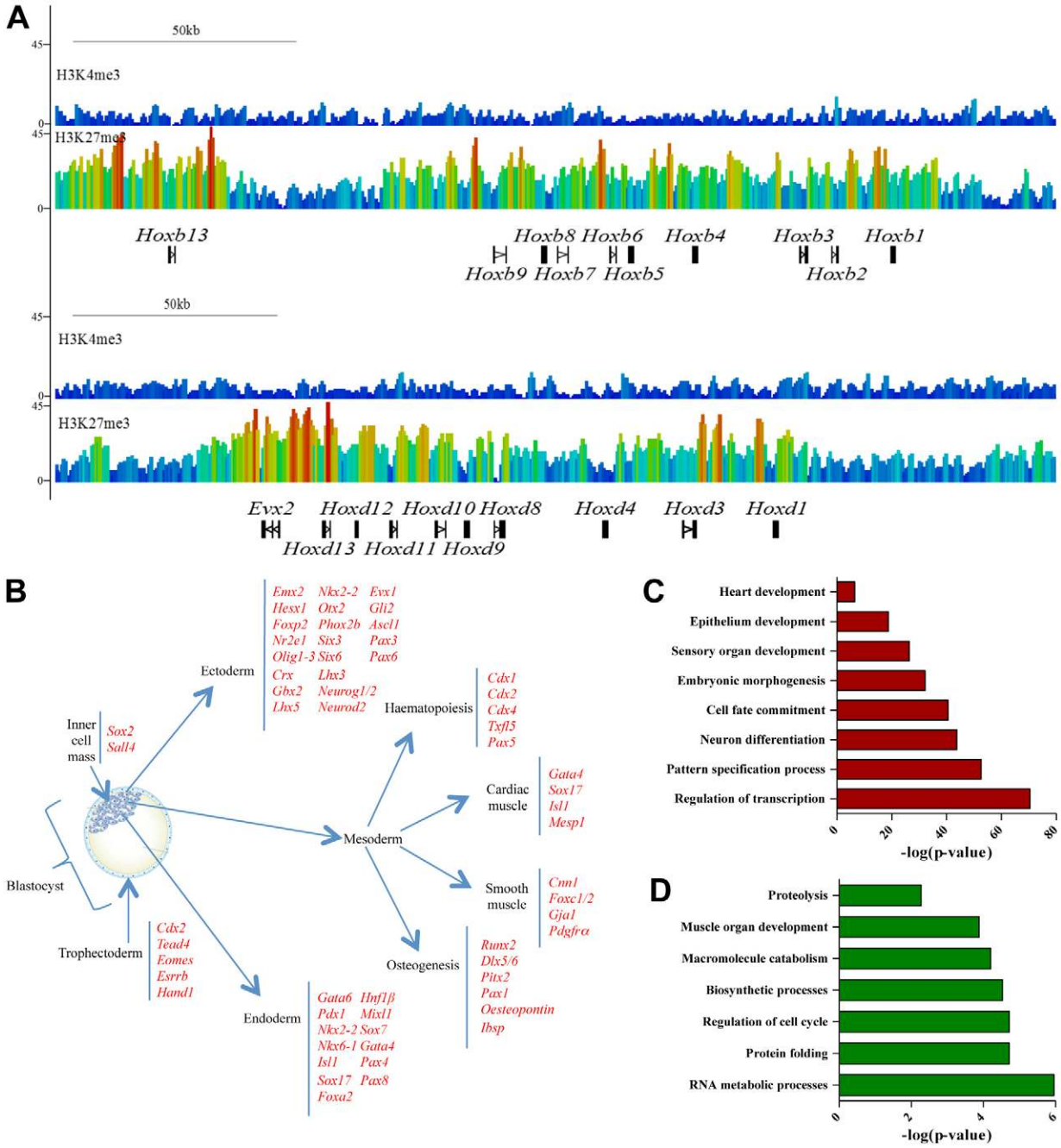

Fig. 5. H3K27me3 marks regulators of cell fate. (**A**) Read-density plot for *Hoxb* and *Hoxd* clusters. Peaks indicate read density. (**B**) Schematic indicating a representative selection of lineage commitment genes marked by H3K27me3; genes are grouped according to the germ layers in which they function. (**C**,**D**) Gene ontology (GO) analysis for the 500 most enriched H3K27me3 (C) H3K4me3 (D) genes, performed using DAVID annotation clustering; representative GO categories are shown and are plotted against −log (p-value).

Thus, Ezh2 does not suppress the muscle differentiation programme in satellite cells.

Discussion

During muscle development, progenitor cells undergo multiple rounds of cell fate restriction, ultimately leading to the creation of lineage-committed satellite cells. By mapping the genome-wide pattern of H3K27me3 in freshly isolated satellite cells, we have identified that a considerable number of key developmental factors involved in fate choice and lineage commitment are marked by this repressive histone modification. These data, combined with the characterisation of two conditional knockout mouse models, outline the critical roles for Ezh2 within satellite cells: to suppress a subset of regulators of non-muscle cell fate, and to ensure appropriate progenitor cell expansion prior to the onset of terminal differentiation.

Utilising the above strategy we have conclusively shown that H3K27me3 marks genes associated with alternative lineage

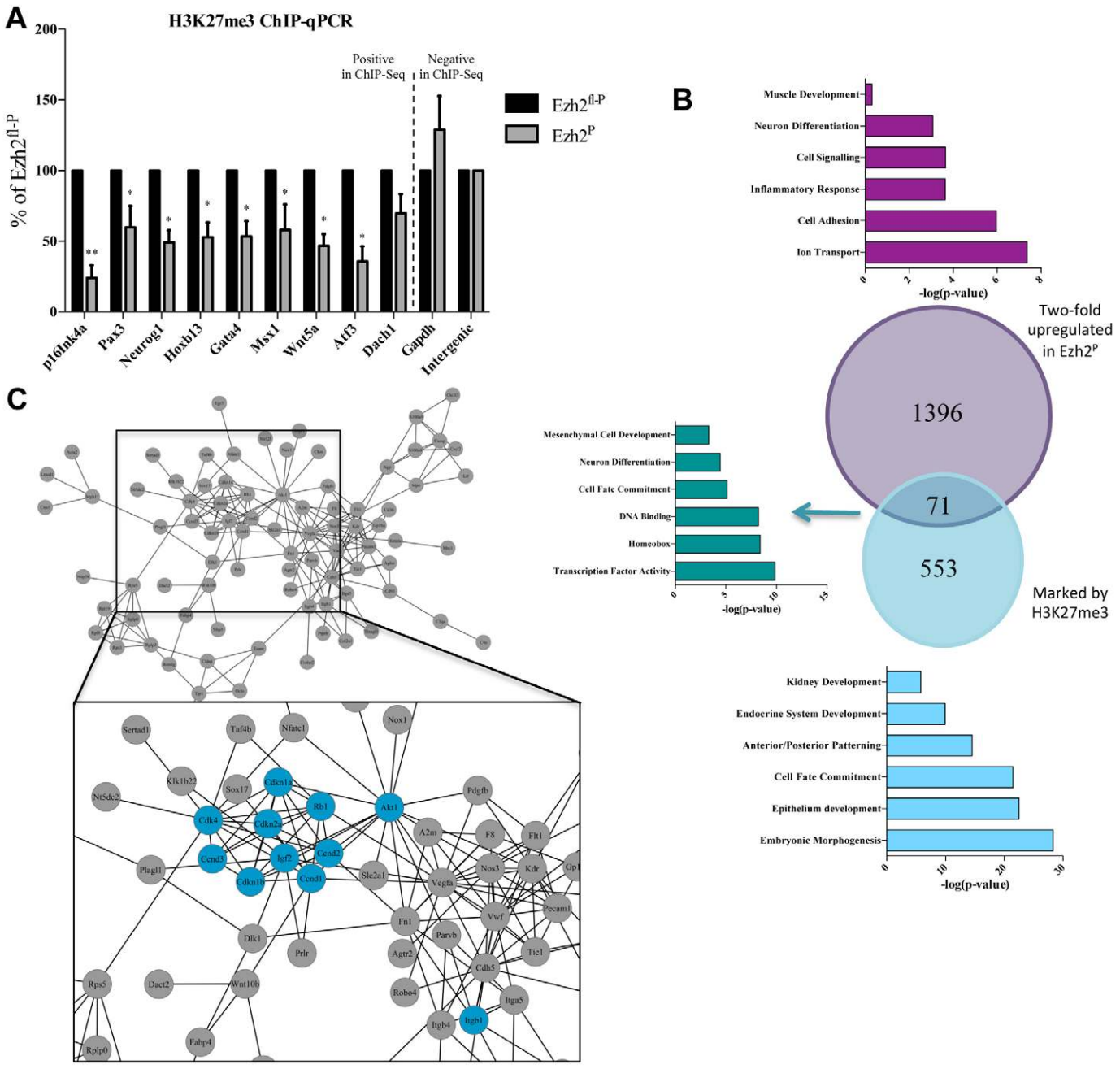

Fig. 6. Transcriptome changes in Ezh2-null satellite cells. (**A**) H3K27me3 ChIP-qPCR for indicated gene promoters; chromatin was obtained from freshly isolated satellite cells from $Ezh2^{fl\text{-}P}$ and $Ezh2^{P}$ mice; $Ezh2^{P}$ data are represented as a percentage of the $Ezh2^{fl\text{-}P}$ control; means+s.e.m.; $n=4$. $^{**}P<0.01$, $^{*}P<0.05$ using one-sample *t*-test. (**B**) Venn diagram indicating overlap of transcripts, identified by RNA-Seq, upregulated greater than twofold in $Ezh2^{P}$ satellite cells when compared with $Ezh2^{fl\text{-}P}$ satellite cells (purple circle); genes (identified by Chip-Seq on $Ezh2^{fl\text{-}P}$ satellite cells) containing greater than 4-fold enrichment of H3K27me3 when compared with input (light blue circle). Overlap between two data sets is highlighted in darker blue. Bar charts indicate representative GO terms on analysis performed for each group. (**C**) Network analysis on upregulated ($P<0.05$) transcripts and their interactors (defined by STRING analysis). Factors involved in cell cycle progression are marked in blue.

choice, but that it does not suppress skeletal muscle terminal differentiation. *Myogenin*, *Ckm* and *MhcIIb* have been identified as key effectors of Ezh2 function in the C2C12 cell line (Asp et al., 2011; Caretti et al., 2004; Juan et al., 2009; Seenundun et al., 2010). However, we have determined that muscle terminal differentiation genes are not marked by H3K27me3 in satellite cells. Furthermore, loss of Ezh2 did not lead to an upregulation of the expression of these genes, and Ezh2 null satellite cells did not spontaneously differentiate [as would have been predicted if master regulators of terminal differentiation (e.g. Myogenin) were expressed]. This disparity between C2C12 cells and satellite cells could be due to several factors. C2C12 cells are immortalised myoblasts that are highly proliferative [they do not contain an intact *Cdkn2a* locus (Pajcini et al., 2010)]. They

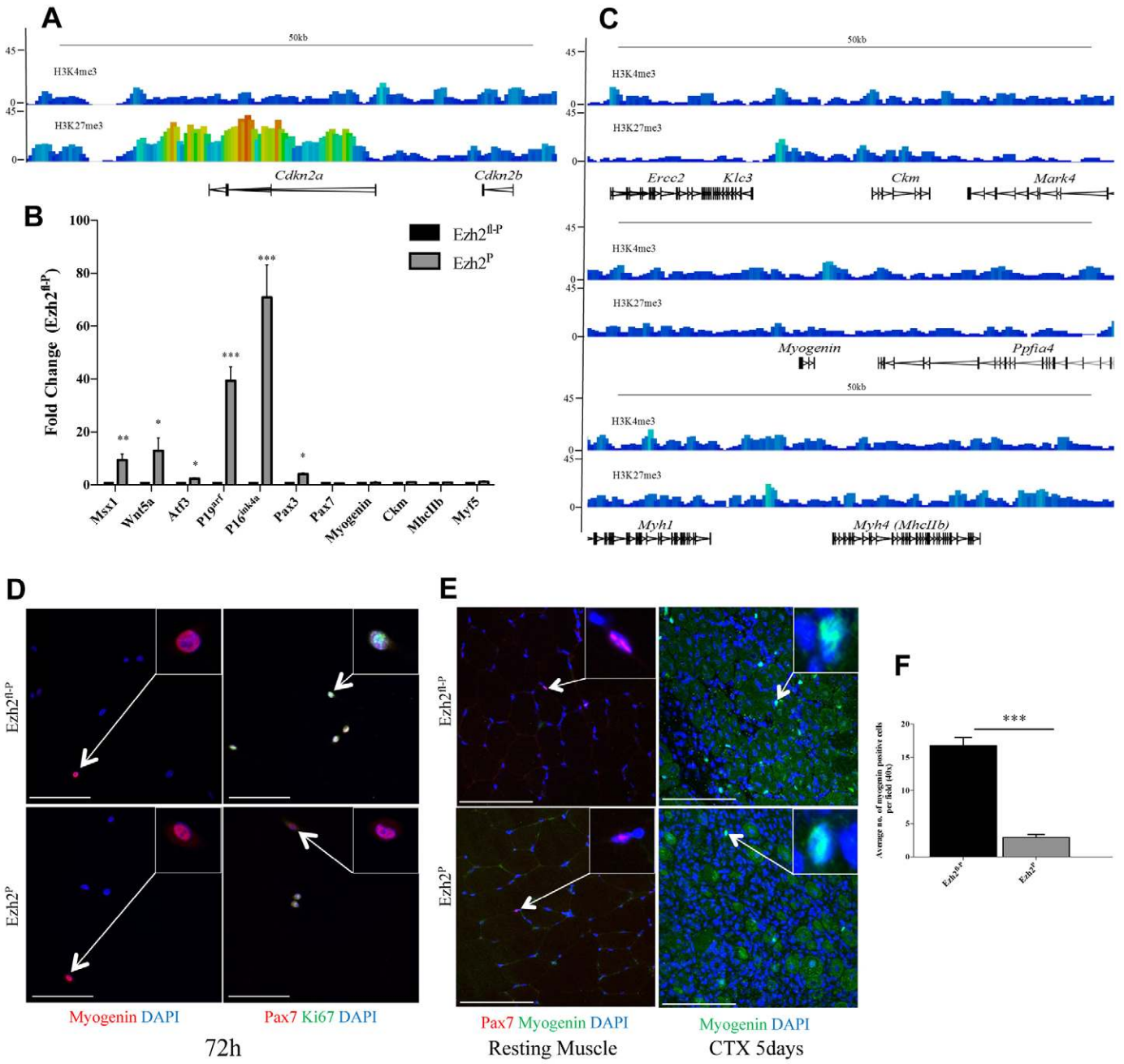

Fig. 7. Ezh2 does not regulate muscle terminal differentiation genes. (**A**) Read-density plots for *Cdkn2a*; peaks indicate read density. (**B**) RT-qPCR for indicated transcripts. mRNA obtained from freshly isolated satellite cells from $Ezh2^{fl\text{-}P}$ and $Ezh2^{P}$ mice, normalised to Rpl32 and 18S; $Ezh2^{P}$ data are represented as a fold change relative to the $Ezh2^{fl\text{-}P}$ control; means+s.e.m.; $n=4$. ***$P<0.001$, **$P<0.01$, *$P<0.05$ assessed using a one-sample *t*-test. (**C**) Read-density plots for *Ckm*, *Myogenin* and *Myh4*; peaks indicate read density. (**D**) FACS-isolated satellite cells cultured for 72 h, stained for Myogenin and Ki67; nuclei were counterstained with DAPI (blue). Scale bars: 100 µm. (**E**) Cross-section of a resting (undamaged) and damaged (5 days after cardiotoxin injection) TA muscle stained for Pax7 (progenitor cells) and Myogenin (marks terminally differentiating cells), as indicated; nuclei are counterstained with DAPI (blue); higher-magnification images indicate $Myogenin^{+/-}$ nuclei. Scale bars: 100 µm. (**F**) Quantification of the number of terminally differentiating myoblasts ($Myogenin^{+}$), average number of $Myogenin^{+}$ nuclei per field of view (40×); means+s.e.m.; $n=3$. ***$P<0.001$, assessed by Student's *t*-test.

are also a heterogeneous population (Olguin and Olwin, 2004). For example, the master regulator of satellite cells, Pax7 (Lepper et al., 2009; Seale et al., 2000) is only expressed in 50% of the cell population (supplementary material Fig. S4D) and (Olguin and Olwin, 2004). In addition, regulators of adipogenesis and osteogenesis, *C/EBP*, *PPAR-y* and *Runx2*, are all marked by the active H3K4me3 mark in C2C12 cells (Asp et al., 2011) but were not marked in satellite cells (supplementary material Table S1). Thus, the H3K27me3 enriched promoters that have been identified within the C2C12 cell line may only exist in a subpopulation of C2C12 cells, and these may not be of true myogenic lineage.

When Ezh2 was ablated via the Pax7 promoter, we observed a significant failure in progenitor myoblast expansion, which resulted in regeneration defects and accumulation of non-muscle tissue. This was not observed when Ezh2 was deleted during terminal differentiation ($Ezh2^{M}$). Utilisation of the Pax7-Cre can lead to Cre-mediated recombination within the central nervous system (Jostes et al., 1990). However, the satellite cell expansion phenotype was also observed *ex vivo*, and deletion of Ezh2 with a MyoD-Cre, which is specific to activated satellite cells, has shown a similar phenotype to that of the $Ezh2^{P}$ strain. Therefore, the muscle defects observed in the $Ezh2^{P}$ strain are likely to result from the loss of Ezh2 within the muscle lineage. However, we cannot exclude the possibility that the growth defects and postnatal lethality observed in the $Ezh2^{P}$ line may occur, in part, due to central nervous system defects.

Even after severe regenerative stimulus, no decline in the number of quiescent satellite cells could be detected in the $Ezh2^{P}$ muscle. Thus, the magnitude of proliferation and differentiation of progenitor populations during muscle regeneration may not influence the replenishment of the satellite cell pool. This notion agrees with the identification of a population of asymmetrically dividing satellite cells that maintains the stem cell pool but does not undergo expansion during regeneration (Kuang et al., 2007; Le Grand et al., 2009). A limited regenerative response was observed in the $Ezh2^{P}$ line and a small number of differentiating myoblasts were present during regeneration. Ezh2 null satellite cells are therefore still capable of differentiation, but it appears that the expansion of progenitor cells is impeded, and the supply of differentiating myoblasts is consequently reduced, leading to a very limited regenerative response.

Within pancreatic islet β cells (Chen et al., 2009) and epidermal basal cells (Ezhkova et al., 2009), the regulation of $p16^{Ink4a}$ by Ezh2 had a powerful influence on proliferation and was shown to directly regulate the expansion of progenitor populations. This common function of Ezh2 also occurs within satellite cells, with a 60-fold upregulation of $p16^{Ink4a}$ in Ezh2 null satellite cells. Indeed, knockdown of $p16^{Ink4a}$ can rescue some of the proliferation defects observed in Ezh2 null satellite cells (Juan et al., 2011). Interestingly, $p16^{Ink4a}$ was the only cyclin dependent kinase inhibitor marked by H3K27me3 in satellite cells. However, RNA-Seq analysis indicates that $p16^{Ink4a}$ may be part of a network of factors that regulate cell cycle progression in Ezh2 null satellite cells.

RNA-Seq analysis of the Ezh2 null satellite cells indicated that even though a large number of developmental regulators are marked by H3K27me3, only a subset of these factors become expressed upon the loss of Ezh2. H3K27me3 is therefore fundamental for regulating a subset of target loci, but at a number of loci, Ezh2 is not required for gene repression. It is tantalising that the factors not upregulated upon loss of Ezh2, are associated with very distant lineages (i.e. epithelium) from that of skeletal muscle. It is possible that these factors are 'permanently' suppressed by layers of epigenetic modifications, which may include DNA methylation and H3K9me3 (Henikoff and Shilatifard, 2011). However, some factors such as *Pax3* and *Cdkn2a*, are upregulated upon the loss of Ezh2, and thus, H3K27me3 may be a dominant mark regulating their expression. Importantly, we have demonstrated that specific developmental factors targeted and suppressed by PRC2 appear to be highly dependent on stem cell lineage.

The maintenance of transcriptional repression is not only important for stem cell function but for tissue integrity in general. For example, mis-expression of the transcription factors *Msx1* and *Twist1* (marked by H3K27me3 in satellite cells) in adult myofibres, results in their de-differentiation and loss of tissue integrity (Hjiantoniou et al., 2008; Kumar et al., 2004; Odelberg et al., 2000). Evidence from the C2C12 cell line and from cultured satellite cells has suggested that Ezh2 may regulate gene repression at the onset of, and during, terminal differentiation (Asp et al., 2011; Palacios et al., 2010). However, we did not observe a skeletal muscle phenotype upon deletion of Ezh2 at the onset of myoblast terminal differentiation *in vivo*, despite a global reduction in H3K27me3 levels. Our work supports the growing body of evidence suggesting that Ezh2 functions within highly proliferative progenitor cell populations (Chen et al., 2009; Ezhkova et al., 2011; Ezhkova et al., 2009; Margueron et al., 2009; Su et al., 2003), as opposed to terminally differentiated tissues or quiescent stem cells. The dependency on Ezh2 during the proliferative phase may reflect the necessity to pass on the information contained within the histone code through multiple cell divisions, which requires the faithful copying of the histone code to progeny during mitosis (Hansen et al., 2008; Petruk et al., 2012). In post-mitotic tissues and quiescent cells it is not necessary for the histone code to be copied and therefore these cell types may not require the actions of Ezh2.

We have identified the developmental window in which Ezh2 acts in the muscle lineage and established that it does not regulate the terminal differentiation process. Instead, Ezh2 promotes satellite cell expansion, ensuring that a critical mass of progenitor cells is achieved prior to the commitment to terminal differentiation. By characterising target loci marked by H3K27me3 and H3K4me3, the study presented here enhances our understanding of the mechanisms that define adult stem cell identity. Determining how tissue specific stem cells are restricted to a particular fate choice may enable greater understanding of the mechanisms underlying stem cell self-renewal, and would aid the use of satellite cells for tissue regeneration, such as in muscular dystrophies.

Materials and Methods

Mouse strains

To conditionally delete Ezh2, mice containing floxed alleles of the SET domain of *Ezh2* (Su et al., 2003), provided by Alexander Tarakhovsky (Rockefeller University), were crossed with mice expressing either Pax7-Cre (Keller et al., 2004) [provided by Mario Capecchi (University of Utah)] or Myogenin-Cre [provided by Eric Olson (University of Texas)]. The Pax7-Cre transgene was used to delete Ezh2 within the satellite cell lineage, while the Myogenin-Cre ensured deletion of Ezh2 upon the initiation of differentiation. All mice were homozygous for the *Ezh2* flox alleles with ($Ezh2^{P}$ or $Ezh2^{M}$) or without ($Ezh2^{fl\text{-}P}$ or $Ezh2^{fl\text{-}M}$) one copy of the Pax7-Cre or Myogenin-Cre transgene. All experiments were performed on mice 7–9 weeks of age [satellite cells are quiescent at this time point (Fukada et al., 2007)] and compared with littermate controls. For CTX-induced muscle regeneration, mice were killed at 5, 10 or 25 days after injection of 100 µl CTX (10 µM; cardiotoxin) or 100 µl PBS (vehicle control) into the tibialis anterior (TA) muscle. All mouse husbandry and experiments were carried out according to the Babraham Institute animal ethics committee under the terms of the UK Home Office.

FACS isolation of satellite cells

To isolate satellite cells, dissected hind limb muscles were digested in 0.25% collagenase type II (Lorn Labs) and 0.2% Dispase II (Roche) in DMEM for 90 min at 37℃ with agitation. Satellite cells were mechanically dissociated from myofibres, by passing the tissue suspension through a 19-gauge needle. These cells were purified by fluorescent activated cell sorting on a FACSAria II (BD Biosciences). Antibodies used were CD31-PE (1:100, Abcam), CD45-PE (1:100,

B.D. Biosciences), CD34-AF647 (1:33, eBiosciences), Vcam1-biotin (1:15, B.D. Biosciences) and Streptavidin-AF488 (1:15, Invitrogen). Dead cells and debris were excluded by DAPI staining and by gating on forward and side scatter profiles. Cells were gated for the $Vcam1^+$ $CD31^-$ and $CD45^-$ population; the satellite cell population was further enriched by gating on $CD34^+$ cells. The final population was $Vcam1^+$, $CD34^+$, $CD31^-$ and $CD45^-$. Satellite cells were cultured in high serum medium (20% FBS, 1% L-glutamine and 1× antibiotic antimycotic solution in DMEM) supplemented with basic FGF (2.5 ng/ml, Promega).

RT-qPCR

Total RNA was isolated from 3×10^5 FACS purified satellite cells with TRIzol reagent (Invitrogen) and cDNA synthesis was performed using the Quantitect Reverse Transcriptase kit (Qiagen). Quantitative real-time PCR was performed using SYBR Green Jumpstart qPCR Mix (Sigma). Expression levels were normalised to Rpl32 (60 s ribosomal protein L32) and 18 s (18 rRNA). RT-qPCR primers are detailed in supplementary material Table S5.

Chromatin immunoprecipitation

ChIP was carried out using ChIP grade antibodies, H3K27me3 (07-499, Millipore) and H3K4me3 (pAB-003-050, Diagenode). ChIP was performed essentially as previously described (Adli et al., 2010). Briefly, freshly isolated satellite cells (5×10^5) or C2C12 cells (8×10^5) were fixed in 4% formaldehyde for 10 min at room temperature and fixation quenched with 150 mM glycine. Chromatin was sheared by sonication to an average fragment size of between 200 and 300 bp using a Bioruptor sonication instrument (Diagenode). Immunoprecipitation was performed using Protein A DynaBeads (Invitrogen). The beads were washed three times with 900 µl of each of the following buffers at 4℃: RIPA buffer, Radioimmunoprecipitation assay buffer, (10 mM Tris-HCl pH 7.5; 140 mM NaCl; 1 mM EDTA; 0.5 mM EGTA; 1% [v/v] Triton X-100; 0.1% [w/v] SDS; 0.1% [w/v] Na-deoxycholate; 10 mM NaF; 1 mM $NaVO_3$; 5 µg/ml aprotinin; 10 µg/ml leupeptin; 1 mM PMSF), high-salt RIPA buffer (RIPA buffer with 500 mM NaCl) and TE (10 mM Tris-HCl pH 8.0; 1 mM EDTA). After reverse crosslinking, enriched DNA fragments were extracted with phenol/chloroform followed by isopropanol precipitation. Immunoprecipitated DNA was either analysed by real-time qPCR or prepared for sequencing. For ChIP-qPCR, enrichment was quantified by real-time qPCR as a percentage of input DNA and represented as a fold change relative to a control region. Primers employed in this study are detailed in supplementary material Table S5.

ChIP-Seq

For ChIP-seq analysis, 4×10^6 freshly sorted satellite cells were collected and pooled from ten independent FACS experiments (160 male mice in total); 2×10^6 satellite cells were used per ChIP. Subsequently, the DNA was adaptor-ligated, amplified using standard protocols (Quail et al., 2008) and sequenced using an Illumina Genome Analyzer GAIIx. H3K4me3-ChIP, H3K27me3-ChIP and input DNA sequence reads were aligned to the mouse genome (assembly NCBIM37/mm9), excluding non-uniquely mapping, and duplicate reads. All analyses were performed using SeqMonk (http://www.bioinformatics.bbsrc.ac.uk/projects/seqmonk/). For identification of peaks, probes (360–2000 bp in length) were designed with a 5-fold enrichment over a random data set and only peaks with a read density that was 4-fold higher than the input were counted. Bivalent domains were defined as containing a H3K27me3 peak (as described above) within 2 kb of a H3K4me3 enriched (4-fold higher than input) promoter. GO analysis was performed using DAVID (Huang et al., 2008).

RNA-Seq

Total RNA was extracted from FACS sorted satellite cells using TRIzol reagent, the quality and the quantity of RNA was checked using Agilent Bioanalyser. Libraries for RNA-Seq were made using Illumina Truseq kit v2 (as per the manufacturer's instructions) and these were then sequenced using Illumina HiSeq. The sequences were then aligned to the mouse genome (NCBIM37/mm9). Three independent replicates, using eight mice per replicate, were used for both $Ezh2^{fl\text{-}P}$ and $Ezh2^{P}$ lines. Further analysis and normalization was performed using Seqmonk. Lists of differentially regulated genes were generated using either a statistical significance test ($P<0.05$) or an intensity difference test ($\log_2$ fold change) for the average of three replicates. Network analysis of differentially regulated genes was performed using STRING (Jensen et al., 2009) and Cytoscape (Cline et al., 2007).

Immunofluorescence and histology

Immunofluorescence on cultured C2C12 cells and satellite cells was performed as previously described (Paxton et al., 2011). TA muscles were harvested and snap frozen in liquid-nitrogen-cooled isopentane, mounted in OCT and 10 µm cryosections collected. Histological analysis was performed using haematoxylin and eosin (morphological analysis), Van Gieson (fibrous tissue), Oil Red O (fatty deposits) or Alizarin Red (calcium deposits) staining using standard histological protocols. For immunofluorescence, cryosections were fixed using 4% paraformaldehyde (PFA) for 10 min, and permeabilised using 0.2% Triton X/PBS. Endogenous IgG was blocked using the MOM kit (Vector Labs). The cryosections were further blocked with 5% goat serum and 3% BSA in 0.2% Triton X/PBS. Both tissue sections and cultured myoblasts were incubated with primary antibodies overnight at 4℃.

Brightfield images were acquired using a Qimaging micro publisher 3.3RTV camera mounted on an Olympus BX41 microscope. For postnatal fibre size analysis, immunofluorescence for laminin (α-2 chain) was used to mark myofibre boundary, and cross sectional area was calculated using ImageJ software (NIH). Fibre types were identified by immunofluorescence with antibodies specific for MyHC subtypes. Total fibre number was quantified, with the aid of Image J (NIH), from tiled images of H and E stained cross-sections of the TA muscle.

The primary antibodies were incubated overnight at 4℃. The antibodies used were: Pax7 (DSHB), MyoD (Santa Cruz Biotechnology), Laminin α-2 chain (Enzo Life Sciences), Myogenin (Santa Cruz Biotechnology), Skeletal Fast Myosin (Sigma), Skeletal Slow Myosin (Sigma), pH 3 Ser10 (Cell Signaling Technology), Ki67 (Leica), Ezh2 (Cell Signaling Technology), M-cadherin (Santa Cruz Biotechnology) and Cleaved Caspase 3 (Cell Signaling Technology).

Secondary antibodies used were donkey anti-rabbit AF488, goat anti-mouse (IgG1 specific) AF568 and goat anti-rat AF633 (Invitrogen). These were added at a dilution of 1:300 for 1 h at room temperature together with DAPI to label nuclei. Slides were mounted with Vectashield hardset (Vector Labs).

Statistical analysis

For all quantitative analyses presented, a minimum of three replicates were performed. Data are presented as means±s.e.m. ANOVA with post-hoc tests and Student's *t*-tests were performed as appropriate (indicated in the figure legends). Statistical analysis was carried out using GraphPad Prism.

Acknowledgements

We thank Alexander Tarakhovsky, Mario Capecchi and Eric Olson for the transgenic mice strains. We are grateful to Peter Rugg-Gunn for critical reading of the manuscript and helpful discussions. The GAIIX sequencing was performed by Kristina Tabbada. Sequencing analysis was performed with the help and advice of Simon Andrews and Felix Krueger. The authors declare that they have no conflict of interest.

Funding

We thank the Biotechnology and Biological Sciences Research Council (BBSRC) for competitive strategic funding to J.M.P. via the Babraham Institute, studentship funding for S.W. and P.B., and Responsive Mode funding [grant number BB-H019243-1 to D.P. and J.M.P.].

Supplementary material available online at
http://jcs.biologists.org/lookup/suppl/doi:10.1242/jcs.114843/-/DC1

References

Adli, M., Zhu, J. and Bernstein, B. E. (2010). Genome-wide chromatin maps derived from limited numbers of hematopoietic progenitors. *Nat. Methods* **7**, 615-618.

Agger, K., Cloos, P. A. C., Rudkjaer, L., Williams, K., Andersen, G., Christensen, J. and Helin, K. (2009). The H3K27me3 demethylase JMJD3 contributes to the activation of the INK4A-ARF locus in response to oncogene- and stress-induced senescence. *Genes Dev.* **23**, 1171-1176.

Asp, P., Blum, R., Vethantham, V., Parisi, F., Micsinai, M., Cheng, J., Bowman, C., Kluger, Y. and Dynlacht, B. D. (2011). Genome-wide remodeling of the epigenetic landscape during myogenic differentiation. *Proc. Natl. Acad. Sci. USA* **108**, E149-E158.

Barradas, M., Anderton, E., Acosta, J. C., Li, S., Banito, A., Rodriguez-Niedenführ, M., Maertens, G., Banck, M., Zhou, M.-M., Walsh, M. J. et al. (2009). Histone demethylase JMJD3 contributes to epigenetic control of INK4a/ARF by oncogenic RAS. *Genes Dev.* **23**, 1177-1182.

Barski, A., Cuddapah, S., Cui, K., Roh, T.-Y., Schones, D. E., Wang, Z., Wei, G., Chepelev, I. and Zhao, K. (2007). High-resolution profiling of histone methylations in the human genome. *Cell* **129**, 823-837.

Benoit, Y. D., Lepage, M. B., Khalfaoui, T., Tremblay, E., Basora, N., Carrier, J. C., Gudas, L. J. and Beaulieu, J. F. (2012). Polycomb repressive complex 2 impedes intestinal cell terminal differentiation. *J. Cell Sci.* **125**, 3454-3463.

Bernstein, B. E., Mikkelsen, T. S., Xie, X., Kamal, M., Huebert, D. J., Cuff, J., Fry, B., Meissner, A., Wernig, M., Plath, K. et al. (2006). A bivalent chromatin structure marks key developmental genes in embryonic stem cells. *Cell* **125**, 315-326.

Boyer, L. A., Plath, K., Zeitlinger, J., Brambrink, T., Medeiros, L. A., Lee, T. I., Levine, S. S., Wernig, M., Tajonar, A., Ray, M. K. et al. (2006). Polycomb complexes repress developmental regulators in murine embryonic stem cells. *Nature* **441**, 349-353.

Brack, A. S., Conboy, I. M., Conboy, M. J., Shen, J. and Rando, T. A. (2008). A temporal switch from notch to Wnt signaling in muscle stem cells is necessary for normal adult myogenesis. *Cell Stem Cell* **2**, 50-59.

Caretti, G., Di Padova, M., Micales, B., Lyons, G. E. and Sartorelli, V. (2004). The Polycomb Ezh2 methyltransferase regulates muscle gene expression and skeletal muscle differentiation. *Genes Dev.* **18**, 2627-2638.

Chamberlain, S. J., Yee, D. and Magnuson, T. (2008). Polycomb repressive complex 2 is dispensable for maintenance of embryonic stem cell pluripotency. *Stem Cells* **26**, 1496-1505.

Chen, H., Gu, X., Su, I. H., Bottino, R., Contreras, J. L., Tarakhovsky, A. and Kim, S. K. (2009). Polycomb protein Ezh2 regulates pancreatic β-cell Ink4a/Arf expression and regeneration in diabetes mellitus. *Genes Dev.* **23**, 975-985.

Cline, M. S., Smoot, M., Cerami, E., Kuchinsky, A., Landys, N., Workman, C., Christmas, R., Avila-Campilo, I., Creech, M., Gross, B. et al. (2007). Integration of biological networks and gene expression data using Cytoscape. *Nat. Protoc.* **2**, 2366-2382.

Cui, K., Zang, C., Roh, T.-Y., Schones, D. E., Childs, R. W., Peng, W. and Zhao, K. (2009). Chromatin signatures in multipotent human hematopoietic stem cells indicate the fate of bivalent genes during differentiation. *Cell Stem Cell* **4**, 80-93.

Delgado-Olguín, P., Huang, Y., Li, X., Christodoulou, D., Seidman, C. E., Seidman, J. G., Tarakhovsky, A. and Bruneau, B. G. (2012). Epigenetic repression of cardiac progenitor gene expression by Ezh2 is required for postnatal cardiac homeostasis. *Nat. Genet.* **44**, 343-347.

Duncan, I. M. (1982). Polycomblike: a gene that appears to be required for the normal expression of the bithorax and antennapedia gene complexes of Drosophila melanogaster. *Genetics* **102**, 49-70.

Ezhkova, E., Pasolli, H. A., Parker, J. S., Stokes, N., Su, I. H., Hannon, G., Tarakhovsky, A. and Fuchs, E. (2009). Ezh2 orchestrates gene expression for the stepwise differentiation of tissue-specific stem cells. *Cell* **136**, 1122-1135.

Ezhkova, E., Lien, W.-H., Stokes, N., Pasolli, H. A., Silva, J. M. and Fuchs, E. (2011). EZH1 and EZH2 cogovern histone H3K27 trimethylation and are essential for hair follicle homeostasis and wound repair. *Genes Dev.* **25**, 485-498.

Faust, C., Schumacher, A., Holdener, B. and Magnuson, T. (1995). The eed mutation disrupts anterior mesoderm production in mice. *Development* **121**, 273-285.

Fukada, S.-i., Uezumi, A., Ikemoto, M., Masuda, S., Segawa, M., Tanimura, N., Yamamoto, H., Miyagoe-Suzuki, Y. and Takeda, S. (2007). Molecular signature of quiescent satellite cells in adult skeletal muscle. *Stem Cells* **25**, 2448-2459.

Guttman, M., Amit, I., Garber, M., French, C., Lin, M. F., Feldser, D., Huarte, M., Zuk, O., Carey, B. W., Cassady, J. P. et al. (2009). Chromatin signature reveals over a thousand highly conserved large non-coding RNAs in mammals. *Nature* **458**, 223-227.

Hansen, K. H., Bracken, A. P., Pasini, D., Dietrich, N., Gehani, S. S., Monrad, A., Rappsilber, J., Lerdrup, M. and Helin, K. (2008). A model for transmission of the H3K27me3 epigenetic mark. *Nat. Cell Biol.* **10**, 1291-1300.

Hawkins, R. D., Hon, G. C., Lee, L. K., Ngo, Q., Lister, R., Pelizzola, M., Edsall, L. E., Kuan, S., Luu, Y., Klugman, S. et al. (2010). Distinct epigenomic landscapes of pluripotent and lineage-committed human cells. *Cell Stem Cell* **6**, 479-491.

Henikoff, S. and Shilatifard, A. (2011). Histone modification: cause or cog? *Trends Genet.* **27**, 389-396.

Hirabayashi, Y., Suzki, N., Tsuboi, M., Endo, T. A., Toyoda, T., Shinga, J., Koseki, H., Vidal, M. and Gotoh, Y. (2009). Polycomb limits the neurogenic competence of neural precursor cells to promote astrogenic fate transition. *Neuron* **63**, 600-613.

Hjiantoniou, E., Anayasa, M., Nicolaou, P., Bantounas, I., Saito, M., Iseki, S., Uney, J. B. and Phylactou, L. A. (2008). Twist induces reversal of myotube formation. *Differentiation* **76**, 182-192.

Huang, D. W., Sherman, B. T. and Lempicki, R. A. (2008). Systematic and integrative analysis of large gene lists using DAVID bioinformatics resources. *Nat. Protoc.* **4**, 44-57.

Jensen, L. J., Kuhn, M., Stark, M., Chaffron, S., Creevey, C., Muller, J., Doerks, T., Julien, P., Roth, A., Simonovic, M. et al. (2009). STRING 8—a global view on proteins and their functional interactions in 630 organisms. *Nucleic Acids Res.* **37**, D412-D416.

Jostes, B., Walther, C. and Gruss, P. (1990). The murine paired box gene, Pax7, is expressed specifically during the development of the nervous and muscular system. *Mech. Dev.* **33**, 27-37.

Juan, A. H., Kumar, R. M., Marx, J. G., Young, R. A. and Sartorelli, V. (2009). Mir-214-dependent regulation of the polycomb protein Ezh2 in skeletal muscle and embryonic stem cells. *Mol. Cell* **36**, 61-74.

Juan, A. H., Derfoul, A., Feng, X., Ryall, J. G., Dell'Orso, S., Pasut, A., Zare, H., Simone, J. M., Rudnicki, M. A. and Sartorelli, V. (2011). Polycomb EZH2 controls self-renewal and safeguards the transcriptional identity of skeletal muscle stem cells. *Genes Dev.* **25**, 789-794.

Keller, C., Hansen, M. S., Coffin, C. M. and Capecchi, M. R. (2004). Pax3:Fkhr interferes with embryonic Pax3 and Pax7 function: implications for alveolar rhabdomyosarcoma cell of origin. *Genes Dev.* **18**, 2608-2613.

Kuang, S., Kuroda, K., Le Grand, F. and Rudnicki, M. A. (2007). Asymmetric self-renewal and commitment of satellite stem cells in muscle. *Cell* **129**, 999-1010.

Kumar, A., Velloso, C. P., Imokawa, Y. and Brockes, J. P. (2004). The regenerative plasticity of isolated urodele myofibers and its dependence on MSX1. *PLoS Biol.* **2**, E218.

Le Grand, F., Jones, A. E., Seale, V., Scimè, A. and Rudnicki, M. A. (2009). Wnt7a activates the planar cell polarity pathway to drive the symmetric expansion of satellite stem cells. *Cell Stem Cell* **4**, 535-547.

Leeb, M., Pasini, D., Novatchkova, M., Jaritz, M., Helin, K. and Wutz, A. (2010). Polycomb complexes act redundantly to repress genomic repeats and genes. *Genes Dev.* **24**, 265-276.

Lepper, C., Conway, S. J. and Fan, C.-M. (2009). Adult satellite cells and embryonic muscle progenitors have distinct genetic requirements. *Nature* **460**, 627-631.

Lepper, C., Partridge, T. A. and Fan, C. M. (2011). An absolute requirement for Pax7-positive satellite cells in acute injury-induced skeletal muscle regeneration. *Development* **138**, 3639-3646.

Li, S., Czubryt, M. P., McAnally, J., Bassel-Duby, R., Richardson, J. A., Wiebel, F. F., Nordheim, A. and Olson, E. N. (2005). Requirement for serum response factor for skeletal muscle growth and maturation revealed by tissue-specific gene deletion in mice. *Proc. Natl. Acad. Sci. USA* **102**, 1082-1087.

Lien, W.-H., Guo, X., Polak, L., Lawton, L. N., Young, R. A., Zheng, D. and Fuchs, E. (2011). Genome-wide maps of histone modifications unwind in vivo chromatin states of the hair follicle lineage. *Cell Stem Cell* **9**, 219-232.

Margueron, R., Li, G., Sarma, K., Blais, A., Zavadil, J., Woodcock, C. L., Dynlacht, B. D. and Reinberg, D. (2008). Ezh1 and Ezh2 maintain repressive chromatin through different mechanisms. *Mol. Cell.* **32**, 503-518.

Margueron, R., Justin, N., Ohno, K., Sharpe, M. L., Son, J., Drury, W. J., 3rd, Voigt, P., Martin, S. R., Taylor, W. R., De Marco, V. et al. (2009). Role of the polycomb protein EED in the propagation of repressive histone marks. *Nature* **461**, 762-767.

Mikkelsen, T. S., Ku, M., Jaffe, D. B., Issac, B., Lieberman, E., Giannoukos, G., Alvarez, P., Brockman, W., Kim, T.-K., Koche, R. P. et al. (2007). Genome-wide maps of chromatin state in pluripotent and lineage-committed cells. *Nature* **448**, 553-560.

Murphy, M. M., Lawson, J. A., Mathew, S. J., Hutcheson, D. A. and Kardon, G. (2011). Satellite cells, connective tissue fibroblasts and their interactions are crucial for muscle regeneration. *Development* **138**, 3625-3637.

O'Carroll, D., Erhardt, S., Pagani, M., Barton, S. C., Surani, M. A. and Jenuwein, T. (2001). The polycomb-group gene Ezh2 is required for early mouse development. *Mol. Cell. Biol.* **21**, 4330-4336.

Odelberg, S. J., Kollhoff, A. and Keating, M. T. (2000). Dedifferentiation of mammalian myotubes induced by msx1. *Cell* **103**, 1099-1109.

Olguin, H. C. and Olwin, B. B. (2004). Pax-7 up-regulation inhibits myogenesis and cell cycle progression in satellite cells: a potential mechanism for self-renewal. *Dev. Biol.* **275**, 375-388.

Pajcini, K. V., Corbel, S. Y., Sage, J., Pomerantz, J. H. and Blau, H. M. (2010). Transient inactivation of Rb and ARF yields regenerative cells from postmitotic mammalian muscle. *Cell Stem Cell* **7**, 198-213.

Palacios, D., Mozzetta, C., Consalvi, S., Caretti, G., Saccone, V., Proserpio, V., Marquez, V. E., Valente, S., Mai, A., Forcales, S. V. et al. (2010). TNF/p38α/polycomb signaling to Pax7 locus in satellite cells links inflammation to the epigenetic control of muscle regeneration. *Cell Stem Cell* **7**, 455-469.

Pan, G., Tian, S., Nie, J., Yang, C., Ruotti, V., Wei, H., Jonsdottir, G. A., Stewart, R. and Thomson, J. A. (2007). Whole-genome analysis of histone H3 lysine 4 and lysine 27 methylation in human embryonic stem cells. *Cell Stem Cell* **1**, 299-312.

Pasini, D., Bracken, A. P., Jensen, M. R., Lazzerini Denchi, E. and Helin, K. (2004). Suz12 is essential for mouse development and for EZH2 histone methyltransferase activity. *EMBO J.* **23**, 4061-4071.

Pasini, D., Bracken, A. P., Hansen, J. B., Capillo, M. and Helin, K. (2007). The polycomb group protein Suz12 is required for embryonic stem cell differentiation. *Mol. Cell. Biol.* **27**, 3769-3779.

Pasini, D., Malatesta, M., Jung, H. R., Walfridsson, J., Willer, A., Olsson, L., Skotte, J., Wutz, A., Porse, B., Jensen, O. N. et al. (2010). Characterization of an antagonistic switch between histone H3 lysine 27 methylation and acetylation in the transcriptional regulation of Polycomb group target genes. *Nucleic Acids Res.* **38**, 4958-4969.

Paxton, C. W., Cosgrove, R. A., Drozd, A. C., Wiggins, E. L., Woodhouse, S., Watson, R. A., Spence, H. J., Ozanne, B. W. and Pell, J. M. (2011). BTB-Kelch protein Krp1 regulates proliferation and differentiation of myoblasts. *Am. J. Physiol. Cell Physiol.* **300**, C1345-C1355.

Pereira, J. D., Sansom, S. N., Smith, J., Dobenecker, M.-W., Tarakhovsky, A. and Livesey, F. J. (2010). Ezh2, the histone methyltransferase of PRC2, regulates the balance between self-renewal and differentiation in the cerebral cortex. *Proc. Natl. Acad. Sci. USA* **107**, 15957-15962.

Petruk, S., Sedkov, Y., Johnston, D. M., Hodgson, J. W., Black, K. L., Kovermann, S. K., Beck, S., Canaani, E., Brock, H. W. and Mazo, A. (2012). TrxG and PcG proteins but not methylated histones remain associated with DNA through replication. *Cell* **150**, 922-933.

Quail, M. A., Kozarewa, I., Smith, F., Scally, A., Stephens, P. J., Durbin, R., Swerdlow, H. and Turner, D. J. (2008). A large genome center's improvements to the Illumina sequencing system. *Nat. Methods* **5**, 1005-1010.

Sacco, A., Doyonnas, R., Kraft, P., Vitorovic, S. and Blau, H. M. (2008). Self-renewal and expansion of single transplanted muscle stem cells. *Nature* **456**, 502-506.

Sambasivan, R., Yao, R., Kissenpfennig, A., Van Wittenberghe, L., Paldi, A., Gayraud-Morel, B., Guenou, H., Malissen, B., Tajbakhsh, S. and Galy, A. (2011). Pax7-expressing satellite cells are indispensable for adult skeletal muscle regeneration. *Development* **138**, 3647-3656.

Schmidt, K., Glaser, G., Wernig, A., Wegner, M. and Rosorius, O. (2003). Sox8 is a specific marker for muscle satellite cells and inhibits myogenesis. *J. Biol. Chem.* **278**, 29769-29775.

Seale, P., Sabourin, L. A., Girgis-Gabardo, A., Mansouri, A., Gruss, P. and Rudnicki, M. A. (2000). Pax7 is required for the specification of myogenic satellite cells. *Cell* **102**, 777-786.

Seenundun, S., Rampalli, S., Liu, Q.-C., Aziz, A., Palii, C., Hong, S., Blais, A., Brand, M., Ge, K. and Dilworth, F. J. (2010). UTX mediates demethylation of H3K27me3 at muscle-specific genes during myogenesis. *EMBO J.* **29**, 1401-1411.

Shea, K. L., Xiang, W., LaPorta, V. S., Licht, J. D., Keller, C., Basson, M. A. and Brack, A. S. (2010). Sprouty1 regulates reversible quiescence of a self-renewing adult muscle stem cell pool during regeneration. *Cell Stem Cell* **6**, 117-129.

Shen, X., Liu, Y., Hsu, Y.-J., Fujiwara, Y., Kim, J., Mao, X., Yuan, G.-C. and Orkin, S. H. (2008). EZH1 mediates methylation on histone H3 lysine 27 and complements EZH2 in maintaining stem cell identity and executing pluripotency. *Mol. Cell* **32**, 491-502.

Schumacher, A., Faust, C. and Magnuson, T. (1996). Positional cloning of a global regulator of anterior-posterior patterning in mice. *Nature* **383**, 250-253.

Soshnikova, N. and Duboule, D. (2008). Epigenetic regulation of Hox gene activation: the waltz of methyls. *Bioessays* **30**, 199-202.

Su, I. H., Basavaraj, A., Krutchinsky, A. N., Hobert, O., Ullrich, A., Chait, B. T. and Tarakhovsky, A. (2003). Ezh2 controls B cell development through histone H3 methylation and Igh rearrangement. *Nat. Immunol.* **4**, 124-131.

Vastenhouw, N. L. and Schier, A. F. (2012). Bivalent histone modifications in early embryogenesis. *Curr. Opin. Cell Biol.* **24**, 374-386.

Wang, Z., Zang, C., Rosenfeld, J. A., Schones, D. E., Barski, A., Cuddapah, S., Cui, K., Roh, T.-Y., Peng, W., Zhang, M. Q. et al. (2008). Combinatorial patterns of histone acetylations and methylations in the human genome. *Nat. Genet.* **40**, 897-903.

White, R. B., Biérinx, A. S., Gnocchi, V. F. and Zammit, P. S. (2010). Dynamics of muscle fibre growth during postnatal mouse development. *BMC Dev. Biol.* **10**, 21.

Young, M. D., Willson, T. A., Wakefield, M. J., Trounson, E., Hilton, D. J., Blewitt, M. E., Oshlack, A. and Majewski, I. J. (2011). ChIP-seq analysis reveals distinct H3K27me3 profiles that correlate with transcriptional activity. *Nucleic Acids Res.* **39**, 7415-7427.

Zhao, X. D., Han, X., Chew, J. L., Liu, J., Chiu, K. P., Choo, A., Orlov, Y. L., Sung, W.-K., Shahab, A., Kuznetsov, V. A. et al. (2007). Whole-genome mapping of histone H3 Lys4 and 27 trimethylations reveals distinct genomic compartments in human embryonic stem cells. *Cell Stem Cell* **1**, 286-298.